Statistics of nodal lines and points in chaotic quantum billiards: perimeter corrections,

fluctuations, curvature

Statistics of nodal lines and points in chaotic quantum billiards: perimeter corrections, fluctuations, curvature

M V Berry

H H Wills Physics Laboratory, University of Bristol, Tyndall Avenue, Bristol BS8 1TL, UK

Abstract

For real (time-reversal symmetric) quantum billiards, the mean length $\langle L \rangle$ of nodal line is calculated for the nth mode ($n \gg 1$), with wavenumber k, using a Gaussian random wave model adapted locally to satisfy Dirichlet or Neumann boundary conditions. The leading term is of order k (i.e. $\sqrt{n}$), and the first (perimeter) correction, dominated by an unanticipated long-range boundary effect, is of order $\log k$ (i.e. $\log n$), with the same sign (negative) for both boundary conditions. The leading-order state-to-state fluctuations δL are of order $\sqrt{\log k}$. For the curvature κ of nodal lines, $\langle |\kappa| \rangle$ and $\sqrt{\langle \kappa^2 \rangle}$ are of order k, but $\langle |\kappa|^3 \rangle$ and higher moments diverge. For complex (e.g. Aharonov–Bohm) billiards, the mean number $\langle N \rangle$ of nodal points (phase singularities) in the mode has a leading term of order k^2 (i.e. n), the perimeter correction (again a long-range effect) is of order $k \log k$ (i.e. $\sqrt{n} \log n$) (and positive, notwithstanding nodal depletion near the boundary) and the fluctuations δN are of order $k \sqrt{\log k}$. Generalizations of the results for mixed (Robin) boundary conditions are stated.

PACS numbers: 05.45.Mt, 03.65.−w, 05.40.−a

1. Introduction

Interest has recently revived in the zeros of quantum wavefunctions of systems that are classically chaotic, in particular as modelled by planar quantum billiards. For systems with time-reversal symmetry, the relevant waves are real, and the zeros are nodal lines (McDonald and Kaufman 1988); these divide the billiard into nodal domains, whose distribution has been studied by Blum *et al* (2002) and Bogomolny and Schmit (2002). In the absence of time-reversal symmetry, for example when the billiard is open or when it is threaded by an Aharonov–Bohm flux line (Berry and Robnik 1986b), the waves are complex and the nodes are points, originally studied in chaotic billiards by Berry and Robnik (1986a), and recently by Saichev *et al* (2002); a wider interest comes from the fact that these point zeros are phase
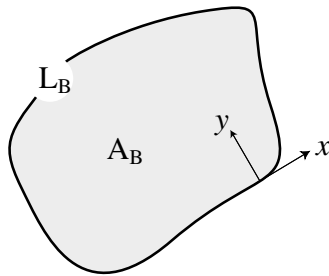
Figure 1. Billiard geometry and local coordinates.

singularities (otherwise called wavefront dislocations, optical vortices or topological charges), on which there is now a large literature (Nye and Berry 1974, Berry 1981, Soskin 1998, Soskin and Vasnetsov 2001a, 2001b, Vasnetsov and Staliunas 1999).

Here I shall study the statistics of nodal lines and points for highly excited chaotic states $n \gg 1$, where the nth state is related to the wavenumber k by the Weyl rule

$$n = \frac{A_B k^2}{4\pi}, \tag{1}$$

where A_B is the area of the billiard (figure 1). The waves will be modelled by Gaussian random functions (Berry 1977), with the innovation that these are adapted to satisfy the boundary conditions locally (section 2). Although the distribution of directions (momenta) of the constituent plane waves is isotropic (reflecting classical ergodicity), the random functions are no longer isotropic: they have different statistics parallel and perpendicular to the boundary. This extension enables the derivation, within the Gaussian random model, of perimeter corrections to the bulk statistics. These corrections are obtained for nodal lines in section 3.1, and for nodal points in section 4.1.

For both lines and points, and both Dirichlet and Neumann boundary conditions, the nodes are repelled by the boundary, locally depleting their density. In addition, there are long-range effects strongly suggesting logarithmic corrections (in k or n) for the billiard as a whole. Surprisingly, these corrections are positive for nodal points, so that the boundary contributes an overall increase in density, notwithstanding the depletion near the boundary. For mixed (Robin) boundary conditions, the analogous results are stated in the appendix.

These boundary corrections to the averages are small effects, and must be compared with the fluctuations to be expected on the isotropic Gaussian random model. These fluctuations are calculated in sections 3.2 and 4.2. Because of long-range behaviour of the relevant correlation functions, the fluctuations are larger than Poisson, and again logarithmic. But they are smaller than the boundary corrections, leading to the hope that the latter will be detected in numerical experiments.

The nodal lines in real waves are curved, and it is possible to calculate the probability distribution of their scalar curvature κ; this calculation, giving a measure of the undulations of the nodal lines, is done in section 3.3. The distribution decays slowly, so that although the averages $\langle|\kappa|\rangle$ and $\langle\kappa^2\rangle$ are finite, $\langle|\kappa^3|\rangle$ and higher moments are infinite.

Real wavefunctions will be denoted by $u(\boldsymbol{r})$, and complex waves by

$$\psi(\boldsymbol{r}) = u(\boldsymbol{r}) + \mathrm{i}v(\boldsymbol{r}), \qquad \boldsymbol{r} = (x, y), \tag{2}$$

where $v(\boldsymbol{r})$ is also real. For Gaussian random functions, the k-dependence is easily extracted by scaling, and it will be convenient to work with the dimensionless coordinates

$$\boldsymbol{R} = (kx, ky) \equiv (X, Y). \tag{3}$$

Where convenient, spatial derivatives will be denoted by subscripts, e.g. u_x or u_y.

For real waves, the quantity whose averages will be calculated is the total length of nodal line in a mode $u(r)$, namely

$$L = \iint_{A_B} d^2r \; \delta(u(r))|\nabla u(r)|. \tag{4}$$

For the complex mode (2), we shall calculate statistics of the total number of nodal points (intersections of nodal lines of u and v), namely (cf Berry and Dennis 2000)

$$N = \iint_{A_B} d^2r \; \delta(u(r))\delta(v(r))|\nabla u(r) \times \nabla v(r)|. \tag{5}$$

The techniques to be used in calculating the nodal statistics are extensions to two-dimensional functions of the classic techniques employed by Rice (1944, 1945) for the zeros of time signals. The first application to phase singularities was by Berry (1978), and a more fully three-dimensional application, together with explanations of the techniques used, was given by Berry and Dennis (2000).

Bies and Heller (2002) have considered a related effect: nodal lines near classical boundaries associated with smooth potentials, rather than the hard walls considered here.

2. Boundary-adapted Gaussian random functions

The familiar Gaussian random function relevant to chaotic quantum billiards is a superposition of plane waves all with the same wavenumber k but different directions. This can be written

$$u_{\text{isotropic}}(\mathbf{R}) = \sqrt{\frac{2}{J}} \sum_{j=1}^{J} \cos(X \cos \theta_j + Y \sin \theta_j + \phi_j), \tag{6}$$

where ϕ_j are random phases and θ_j are random directions, both uniformly distributed in the range 0–2π, and the number of waves is $J \gg 1$, ensuring that linear functionals of u are Gauss distributed. For the complex wave (2), the imaginary part $v(\mathbf{R})$ is given by the formula (6) with the cosine replaced by sine, and the same values of the angles ϕ_j and θ_j.

Such an isotropic superposition does not satisfy prescribed boundary conditions (though of course it satisfies Dirichlet conditions on boundaries determined by its closed nodal lines, which however vary from sample to sample). It is easy, though, to create Gaussian random superpositions that satisfy Dirichlet or Neumann conditions at straight boundaries, and this will be sufficient to establish the leading-order (in k or n) correction to the bulk statistics generated by (6). In a sense this is a statistical counterpart of the procedure employed by Balian and Bloch (1970), who determined the perimeter correction to the Weyl rule (1) by employing free-space Green functions adapted to satisfy conditions on a straight boundary.

With the boundary defined as the x axis (figure 1), the adapted superposition for Dirichlet conditions ($u = 0$ for $y = 0$) is

$$u_{\text{Dirichlet}}(\mathbf{R}) = \frac{2}{\sqrt{J}} \sum_{j=1}^{J} \sin(Y \sin \theta_j) \cos(X \cos \theta_j + \phi_j). \tag{7}$$

For Neumann conditions ($u_y = 0$ for $y = 0$), the corresponding superposition is

$$u_{\text{Neumann}}(\mathbf{R}) = \frac{2}{\sqrt{J}} \sum_{j=1}^{J} \cos(Y \sin \theta_j) \cos(X \cos \theta_j + \phi_j). \tag{8}$$

For complex wavefunctions, the imaginary parts $v(\mathbf{R})$ (equation (2)) are given by the formulae (7) and (8), with the cosines involving X replaced by sines.

All required averages of these functions (denoted $\langle \cdots \rangle$) can be calculated by integrating over ϕ_j and θ_j. In particular, we shall need the following averages for products of u at a given point:

Dirichlet:

$$
\begin{aligned}
\langle u^2 \rangle &= 1 - J_0(2Y) \equiv B_{\text{Dirichlet}} \\
\langle u_X^2 \rangle &= \tfrac{1}{2}(1 - J_0(2Y) - J_2(2Y)) \equiv D_{x,\text{Dirichlet}} \\
\langle u_Y^2 \rangle &= \tfrac{1}{2}(1 + J_0(2Y) - J_2(2Y)) \equiv D_{y,\text{Dirichlet}} \\
\langle u u_Y \rangle &= J_1(2Y) \equiv K_{\text{Dirichlet}},
\end{aligned}
\tag{9}
$$

Neumann:

$$
\begin{aligned}
\langle u^2 \rangle &= 1 + J_0(2Y) \equiv B_{\text{Neumann}} \\
\langle u_X^2 \rangle &= \tfrac{1}{2}(1 + J_0(2Y) + J_2(2Y)) \equiv D_{x,\text{Neumann}} \\
\langle u_Y^2 \rangle &= \tfrac{1}{2}(1 - J_0(2Y) + J_2(2Y)) \equiv D_{y,\text{Neumann}} \\
\langle u u_Y \rangle &= -J_1(2Y) \equiv K_{\text{Neumann}},
\end{aligned}
\tag{10}
$$

and the following averages for products at two different points $\boldsymbol{R}_A$, $\boldsymbol{R}_B$, using coordinates X and Y parallel and perpendicular to $\boldsymbol{R}_A - \boldsymbol{R}_B$ respectively:

Isotropic:

$$
\begin{aligned}
\langle u(\boldsymbol{R}_A) u(\boldsymbol{R}_B) \rangle &= J_0(R) \equiv C \\
(\text{so} \langle u^2(\boldsymbol{R}_A) \rangle &= \langle u^2(\boldsymbol{R}_B) \rangle = 1) \\
\langle u(\boldsymbol{R}_A) u_X(\boldsymbol{R}_B) \rangle &= -\langle u_X(\boldsymbol{R}_A) u(\boldsymbol{R}_B) \rangle = J_1(R) \equiv E \\
\langle u_X(\boldsymbol{R}_A) u_X(\boldsymbol{R}_B) \rangle &= \tfrac{1}{2}(J_0(R) - J_2(R)) \equiv F \\
(\text{so} F_0 &\equiv \langle u_X^2 \rangle = \tfrac{1}{2}) \\
\langle u_Y(\boldsymbol{R}_A) u_Y(\boldsymbol{R}_B) \rangle &= J_1(R)/R \equiv H.
\end{aligned}
\tag{11}
$$

All other relevant correlations vanish, including correlations between the real and imaginary parts u and v; for some quantities, the vanishing follows from averaging over the random phases ϕ_j, while for others it is a consequence of averaging over the angles θ_j.

These correlations are components of probability distributions, which will always be denoted by the generic symbol P, whose arguments will unambiguously specify the variables. Two useful distributions are

$$
P(u_X) = \frac{\exp\left(-u_X^2/2D_X\right)}{\sqrt{2\pi D_X}}, \qquad P(u = 0, u_Y) = \frac{\exp\left(-B u_Y^2/2(B D_Y - K^2)\right)}{2\pi \sqrt{B D_Y - K^2}}.
\tag{12}
$$

These and other distributions can easily be calculated using $\langle \exp(\mathrm{i} f) \rangle = \exp(-\tfrac{1}{2}\langle f^2 \rangle)$ for any linear functional of Gaussian variables with zero mean.

3. Nodal lines

3.1. Mean nodal line length

The average of (4) can be written in the form

$$
\langle L \rangle = \frac{k}{2\sqrt{2}} \iint_{A_B} \mathrm{d}^2 \boldsymbol{r} \, \rho_L(Y)
\tag{13}
$$

where the prefactor is the mean density of nodal length, so that the quantity $\rho_L(Y) \to 1$ as $Y \to \infty$. $\rho_L(Y)$ is the factor modifying the mean density of nodal length as a function of distance from the boundary. This function can be determined as follows:
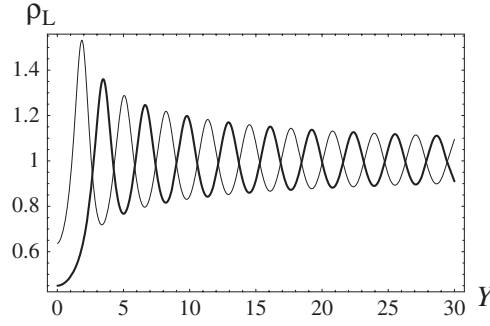
Figure 2. Mean nodal line density $\rho_L(Y)$, for Dirichlet (thick curve) and Neumann (thin curve) boundary conditions.

$$\rho_L(Y) = 2\sqrt{2}\langle\delta(u)|\nabla_R u|\rangle = \frac{1}{\pi^{3/2}\sqrt{D_X(BD_Y - K^2)}}$$

$$\times \int_{-\infty}^{\infty} du_X \int_{-\infty}^{\infty} du_Y \exp\left\{-\frac{1}{2}\left(\frac{u_X^2}{D_X} + \frac{Bu_Y^2}{BD_Y - K^2}\right)\right\}\sqrt{u_X^2 + u_Y^2}$$

$$= \frac{2\sqrt{2}}{\pi}D_X(BD_Y - K^2)\int_0^{\pi/2}\frac{d\theta}{(BD_X\cos^2\theta + (BD_Y - K^2)\sin^2\theta)^{3/2}}, \quad (14)$$

where the first equality follows from (4), the second from the probability distributions (12) and the third from integrating over the $|\nabla u|$; the quantities B, etc, are defined in (9) and (10).

It is possible to evaluate the θ integral in (14) in terms of elliptic functions, but I do not give the expression here. Graphs of $\rho_L(Y)$ for Dirichlet and Neumann boundary conditions, obtained by substituting the correlations (9) or (10), are shown in figure 2. In both cases there is nodal repulsion from the boundary (i.e. $\rho_L(Y) < 1$), stronger for Dirichlet than Neumann, reflecting the fact that for both conditions the nodal lines typically intersect the boundary perpendicularly (non-perpendicular intersections can easily be constructed, but correspond to higher-order, and hence unstable, zeros). In the Dirichlet case, perpendicularity is a consequence of the fact that a boundary nodal intersection is a zero-height saddle of $u(r)$, together with the wave equation, which states that $\nabla^2 u = 0$ when $u = 0$. In the Neumann case, perpendicularity arises because ∇u points along the boundary, so the contours of u, including $u = 0$, are perpendicular to ∇u.

Far from the boundary, $\rho_L(Y)$ decays to 1 while oscillating. The asymptotics of this decay, including the leading-order non-oscillatory term, can be obtained from (14) using the Hankel asymptotics of the Bessel functions in (9) or (10). For Dirichlet conditions, the result is

$$\rho_{L,\text{Dirichlet}}(0) = \frac{\sqrt{2}}{\pi}$$

$$\rho_{L,\text{Dirichlet}}(Y) = 1 + \frac{\cos[2Y - \frac{1}{4}\pi]}{\sqrt{\pi Y}} - \frac{1}{32\pi Y} + O\left(\frac{1}{Y}\right) \qquad \text{as } Y \to \infty. \tag{15}$$

The term $-Y^{-1}$ implies an infinite deficit in mean line length in an infinite strip perpendicular to the boundary. The development of this deficit can be quantified by (negative) excess in a strip of height Y:

$$\int_0^Y dU\,(\rho_{L,\text{Dirichlet}}(U) - 1) = -\frac{\log Y}{32\pi} - 0.945 + \frac{\sin(2Y - \frac{1}{4}\pi)}{2\sqrt{\pi Y}} + O\left(\frac{1}{\sqrt{Y}}\right) \tag{16}$$
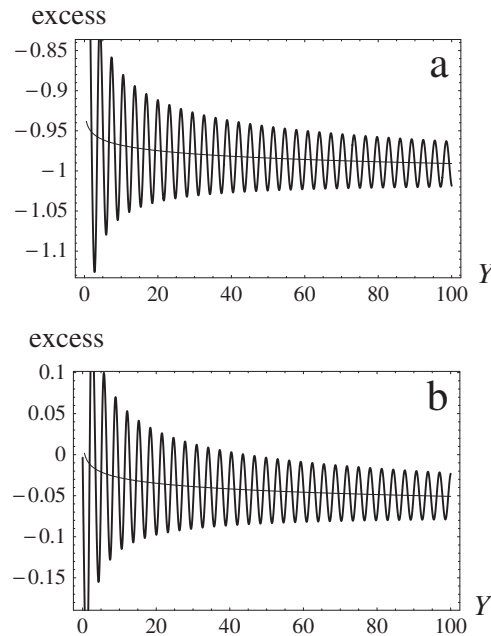
Figure 3. Mean excess nodal line length $\int_0^Y \mathrm{d}U\,(\rho_L(U)-1)$, for (*a*) Dirichlet, (*b*) Neumann boundary conditions. Thick curves, exact; thin curves, nonoscillatory parts of the approximations (16) and (18) (with the oscillatory contributions, the curves cannot be distinguished).

where the constant -0.945 has been determined by numerical integration based on (14). Figure 3(*a*) shows this excess, together with the nonoscillatory part of the asymptotic approximation (16).

For Neumann conditions, the expressions corresponding to (15) and (16) are

$$\rho_{L,\text{Neumann}}(0) = \frac{2}{\pi}$$

$$\rho_{L,\text{Neumann}}(Y) = 1 - \frac{\cos[2Y - \frac{1}{4}\pi]}{\sqrt{\pi Y}} - \frac{1}{32\pi Y} + \mathrm{O}\left(\frac{1}{Y}\right) \qquad \text{as } Y \to \infty \tag{17}$$

and

$$\int_0^Y \mathrm{d}U\,(\rho_{L,\text{Neumann}}(U) - 1) = -\frac{\log Y}{32\pi} - 0.005 - \frac{\sin(2Y - \frac{1}{4}\pi)}{2\sqrt{\pi Y}} + \mathrm{O}\left(\frac{1}{\sqrt{Y}}\right), \tag{18}$$

and the density and excess are displayed in figures 2 and 3(*b*).

To obtain the mean total line length, it is necessary to integrate $\rho_L(Y)$ over the domain A_B according to (13). To separate the bulk and boundary contributions, we write $\rho_L(Y) = 1 + (\rho_L(Y) - 1)$. The term 1 gives the area A_B, and generates the bulk contribution to (13). For the integration over A_B in the boundary term, a natural procedure is to use local coordinates x (parallel to the boundary) and y (perpendicular to the boundary) (figure 1). The integration over x simply gives the perimeter L_B. In the integration over y, the oscillatory terms in (15) or (17) disappear by interference, but the terms in Y^{-1} lead to logarithmic divergences as in (16) or (18). The correct procedure would seem to be to terminate the integration at a y value representing the diameter of the billiard, e.g. $\sqrt{A_B}$, leading to

$$\langle L \rangle = \frac{kA_B}{2\sqrt{2}} - \frac{L_B}{64\pi\sqrt{2}} \log(k\sqrt{A_B}) + \mathrm{O}(k^0). \tag{19}$$

It is interesting that the perimeter correction is the same for both Dirichlet or Neumann conditions, in contrast to the perimeter correction to the Weyl rule (1) for the level counting function, which is negative for the Dirichlet case and positive in the Neumann case.

A convenient way to represent (19) in dimensionless form is to divide L by $\sqrt{A_B}$ and replace k by the level number n according to the Weyl rule (1). This gives

$$\frac{\langle L \rangle}{\sqrt{A_B}} = \sqrt{\frac{\pi n}{2}} - \frac{L_B}{128\pi\sqrt{2A_B}} \log n + \mathrm{O}(n^0). \tag{20}$$

At this level of approximation, the constant term in (19) or (20) is undetermined. The constant depends, for example, on the choice of cutoff for the Y integration, on the choice of Jacobian for the area integration (strictly this should be not $\mathrm{d}x\,\mathrm{d}y$ but $\mathrm{d}x\,\mathrm{d}y(1 - y/R(x))$, where $R(x)$ is the radius of curvature of the boundary at x) and also, in the case of (20), whether the Weyl rule relating k to n includes the perimeter correction.

3.2. Nodal line length fluctuations

Because of statistical fluctuations, the nodal line length will vary from state to state. It is important to estimate the strength of these fluctuations, in case they threaten to mask the boundary corrections (19) and (20). The fluctuations can be represented by

$$\delta L \equiv \sqrt{\langle (L - \langle L \rangle)^2 \rangle} = \sqrt{\langle L^2 - \langle L \rangle^2 \rangle}. \tag{21}$$

To calculate δL according to the Gaussian random model, it suffices to use the isotropic superposition (6). This gives, using (4),

$$\langle L^2 \rangle = \frac{k^2}{8} \iint_{A_B} \mathrm{d}\boldsymbol{r}_A \iint_{A_B} \mathrm{d}\boldsymbol{r}_B \, g_L(|\boldsymbol{R}_A - \boldsymbol{R}_B|), \tag{22}$$

where

$$g_L(|\boldsymbol{R}_A - \boldsymbol{R}_B|) = 8\langle \delta(u(\boldsymbol{r}_A))\delta(u(\boldsymbol{r}_B))|\nabla_R u(\boldsymbol{r}_A)||\nabla_R u(\boldsymbol{r}_B)|\rangle. \tag{23}$$

The factor $k^2/8$ is chosen to ensure that $g_L(R) \to 1$ as $R \to \infty$.

The average in (23) is easier to calculate if the factors $|\nabla u|$ are represented in Gaussian form, and this can be achieved with the identity

$$|\boldsymbol{A}| = \frac{1}{\sqrt{2\pi}} \int_0^\infty \frac{\mathrm{d}t}{t^{3/2}} \left(1 - \exp\left(-\frac{1}{2}\boldsymbol{A} \cdot \boldsymbol{A}t\right)\right). \tag{24}$$

With probability distributions obtained from the correlations (11), the quantity to be averaged involves only Gaussian integrals, leading to

$$g_L(R) = \frac{2}{\pi^2\sqrt{D_1 D_2}} \int_0^\infty \frac{\mathrm{d}t_A}{t_A^{3/2}} \int_0^\infty \frac{\mathrm{d}t_B}{t_B^{3/2}}$$
$$\times \left[\frac{1}{\sqrt{\Delta(0,0)}} - \frac{1}{\sqrt{\Delta(t_A, 0)}} - \frac{1}{\sqrt{\Delta(0, t_B)}} - \frac{1}{\sqrt{\Delta(t_A, t_B)}} \right], \tag{25}$$

where
$$D_1 \equiv [E^2 - (1+C)(F_0 - F)][E^2 - (1-C)(F_0 + F)], \qquad D_2 \equiv F_0^2 - H^2,$$
$$\Delta(t_A, t_B) \equiv [(\gamma + t_A)(\gamma + t_B) - \delta^2][(\alpha + t_A)(\alpha + t_B) - \beta^2],$$
$$\alpha \equiv \frac{1}{D_1}[F_0(1 - C^2) - E^2], \qquad \beta \equiv \frac{1}{D_1}[CE^2 - F(1 - C^2)], \tag{26}$$
$$\gamma \equiv \frac{F_0}{D_2}, \qquad \delta \equiv -\frac{H}{D_2}.$$

I have not been able to evaluate the integrals over t_A and t_B analytically, but to estimate the leading-order fluctuations this is not necessary, since the variable $R = kr \gg 1$ for almost the entire range of the area integrations in (22). Only the large-R asymptotics is required, and this can be established with the aid of the asymptotics of the Bessel functions (including the first correction to the leading-order approximations) occurring in the quantities in (26) (cf (11)); the resulting integrals over t_A and t_B can be evaluated analytically, with the result

$$g_L(R) = 1 + \frac{2\sin(2R)}{\pi R} + \frac{1}{64\pi^2 R^2} + \mathrm{O}\left(\frac{\sin(2R + \mu)}{R^2}\right). \tag{27}$$

The fact that the leading nonoscillatory term is of order R^{-2} rather than R^{-1}, as might have been expected from the asymptotics of squares of Bessel functions, is surprising; it results from a cancellation whose meaning is still obscure.

To evaluate the double integral (22), we use (27), with a lower cutoff at $R \sim 1$ and an upper cutoff at $R \sim k\sqrt{A_B}$, and ignore the oscillatory term because it will cancel by interference. This leads to

$$(\delta L)^2 \approx \frac{A_B}{256\pi} \log(k\sqrt{A_B}) \tag{28}$$

and its dimensionless counterpart

$$\frac{\delta L}{\sqrt{A_B}} \approx \frac{1}{16}\sqrt{\frac{\log n}{2\pi}}. \tag{29}$$

The fluctuations thus calculated are smaller—but only just!—than the boundary contributions (19) and (20). This happy conclusion is the result of the cancellation already mentioned, leading to the smaller-than-expected nonoscillatory term in (27), and gives rise to the hope that the nodal length boundary corrections might be detected in numerical experiments without the need to average over long sequences of states.

3.3. Curvatures of nodal lines

From elementary differential geometry (e.g. Struik 1950), the curvature (rate of turning of the tangent) of a contour line of u at point r is

$$\kappa(r) = \frac{u_x^2 u_{xx} + u_y^2 u_{yy} - 2u_x u_y u_{xy}}{|\nabla u|^3}. \tag{30}$$

Therefore the probability distribution of curvature of nodal lines, weighted according to nodal line length, is

$$P(\kappa) = \frac{\langle \delta(u)|\nabla u|\delta(\kappa - \kappa(r))\rangle}{\langle \delta(u)|\nabla u|\rangle}. \tag{31}$$

To calculate this on the Gaussian random model, it again suffices to use the isotropic superposition (6). For the gradient, it is convenient to use the polar representation

$$\nabla u = |\nabla u|(\cos\theta, \sin\theta). \tag{32}$$

A considerable simplification results from noticing that on a nodal line the wave equation gives $u_{yy} = -u_{xx}$. Then an obvious k scaling gives

$$P\left(\frac{\kappa}{k}\right) = \frac{\left\langle \delta(u)|\nabla_R u|\delta\left(\kappa/k - \left((u_{xx}\cos 2\theta - u_{xy}\sin 2\theta)/|\nabla_R u|\right)\right)\right\rangle}{\langle \delta(u)|\nabla_R u|\rangle}. \tag{33}$$

The relevant additional required averages are

$$\langle |\nabla_R u|^2\rangle = 1, \qquad \langle u_{xx}^2\rangle = \tfrac{3}{8}, \qquad \langle u_{xy}^2\rangle = \tfrac{1}{8}, \qquad \langle uu_{xx}\rangle = -\tfrac{1}{2}, \tag{34}$$

leading to the probability distributions

$$P(|\nabla u|) = 2|\nabla u| \exp(-|\nabla u|^2)$$

$$P(u = 0, u_{xx}) = \frac{\sqrt{2}}{\pi} \exp(-4u_{xx}^2). \tag{35}$$

Evaluation of (33) now requires only elementary integrations, giving the result

$$P\left(\frac{\kappa}{k}\right) = \frac{4}{\pi(1 + (\kappa/k)^2)^2}. \tag{36}$$

This gives the not very surprising result that the radii of curvature of the nodal lines are of the order of the wavelength $\lambda = 2\pi/k$; more precisely,

$$\langle|\kappa|\rangle = \frac{k}{\pi} = \frac{2}{\lambda}, \qquad \sqrt{\langle\kappa^2\rangle} = \frac{k}{2} = \frac{\pi}{\lambda}. \tag{37}$$

However, the long tail of the distribution (36) means that higher moments of κ are infinite, indicating places where nodal lines can be very strongly curved—for example close to places where nodal lines cross (these have codimension 1, see Berry 1983). Similar behaviour occurs in the distribution of curvatures of nodal lines in random complex waves in three dimensions (Berry and Dennis 2000).

The result (36), for the (naturally length-weighted) curvatures of nodal lines, contrasts with the distribution of (naturally area-weighted) curvatures of all u-contours, namely $(1 + 4(\kappa/k)^2/3)^{-3/2}$.

4. Nodal points

4.1. Mean number of nodal points

From (5), the mean number of nodal points is

$$\langle N \rangle = \frac{k^2}{4\pi} \iint_{A_B} \mathrm{d}\boldsymbol{r} \; \rho_P(Y), \tag{38}$$

where, in terms of the complex Gaussian superposition defined by (2), (7) and (8),

$$\rho_P(Y) = 4\pi \langle \delta(u)\delta(v)|\nabla_R u \times \nabla_R v|\rangle. \tag{39}$$

The prefactor is chosen so that $\rho_P(Y) \to 1$ as $R \to \infty$, corresponding to the lowest-order (bulk) mean number $A_B k^2/4\pi$, previously calculated by Berry and Robnik (1986a) and for a wider class of situations (e.g. speckle patterns and black-body radiation) by Berry and Dennis (2000). The averages in (39) are easy to calculate in terms of the quantities defined in (9) and (10), with the result

$$\rho_P(Y) = \frac{2\sqrt{D_X(BD_Y - K^2)}}{B^{3/2}}. \tag{40}$$

Figure 4 shows this density for Dirichlet and Neumann boundary conditions. In both cases, $\rho_P(0) = 0$, indicating repulsion of nodal points from the boundary; this is stronger for Dirichlet than for Neumann, as can be seen from the sample boundary-adapted functions in figure 6.

Notwithstanding this local depletion near the boundary, the asymptotic density eventually exceeds that in the bulk: for large Y, $\rho_P(Y)$ tends to unity from above. For the Dirichlet case,

$$\rho_{P,\text{Dirichlet}}(Y) = 1 + \frac{2\cos[2Y - \frac{1}{4}\pi]}{\sqrt{\pi Y}} + \frac{1}{4\pi Y} + \mathrm{o}\left(\frac{1}{Y}\right) \qquad \text{as } Y \to \infty, \tag{41}$$
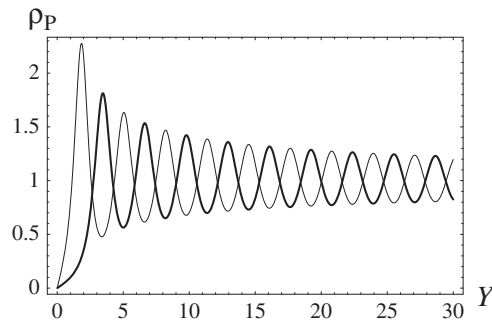
Figure 4. Mean density of nodal points $\rho_P(Y)$, for Dirichlet (thick curve) and Neumann (thin curve) boundary conditions.
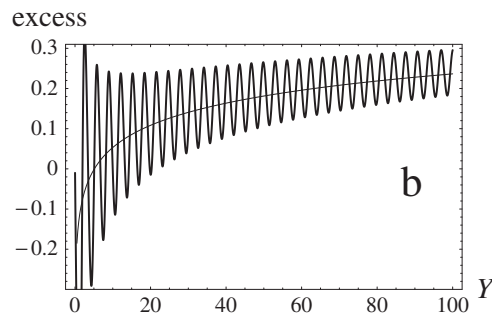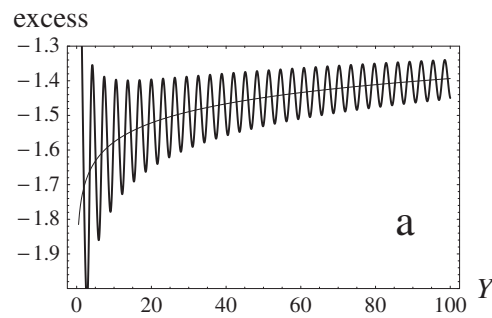

Figure 5. Mean excess of nodal points $\int_0^Y dU \, (\rho_P(U)-1)$, for (a) Dirichlet, (b) Neumann boundary conditions. Thick curves, exact; thin curves, nonoscillatory parts of the approximations (42) and (44) (with the oscillatory contributions, the curves cannot be distinguished).

and the long-range phenomenon just described is indicated by the positivity of the coefficient of Y^{-1}. Moreover, the excess is nonintegrable, with the number of zeros in a unit strip of length Y diverging logarithmically (figure 5(a)) as

$$\int_0^Y dU(\rho_{P,\text{Dirichlet}}(U) - 1) = \frac{\log Y}{4\pi} - 1.76 + \frac{\sin(2Y - \frac{1}{4}\pi)}{\sqrt{\pi Y}} + o\left(\frac{1}{\sqrt{Y}}\right). \tag{42}$$

Again, the coefficient is determined numerically. Its relatively large value indicates that only at the large distance $Y \sim \exp(1.76 \times 4\pi) \sim 4 \times 10^9$ from the boundary does this asymptotic excess compensate the local depletion near $Y = 0$.
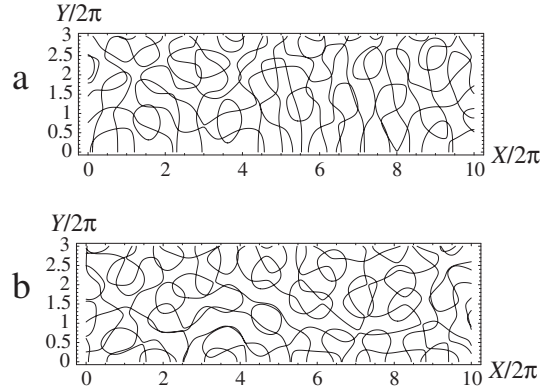
Figure 6. Nodal points of complex wave $\psi(\boldsymbol{R})$ (i.e. intersections of nodal lines of Re ψ and Im ψ), taken from the Gaussian random ensemble: (*a*) Dirichlet (equation (7)) and (*b*) Neumann (equation (8)), with $J = 30$. The boundary is $Y = 0$, and the axes are labelled in wavelength units.

There is a similar asymptotic excess in the Neumann case, with the same positive coefficient of Y^{-1}:

$$\rho_{P,\text{Neumann}}(Y) = 1 - \frac{2\cos[2Y - \frac{1}{4}\pi]}{\sqrt{\pi Y}} + \frac{1}{4\pi Y} + o\!\left(\frac{1}{Y}\right) \qquad \text{as } Y \to \infty. \tag{43}$$

However, in the logarithmic divergence, given by

$$\int_0^Y \mathrm{d}U \left(\rho_{P,\text{Neumann}}(U) - 1\right) = \frac{\log Y}{4\pi} - 0.13 - \frac{\sin(2Y - \frac{1}{4}\pi)}{\sqrt{\pi Y}} + o\!\left(\frac{1}{\sqrt{Y}}\right) \tag{44}$$

(figure 5(*b*)), the coefficient is smaller, so the asymptotic excess should dominate at the much smaller distance $Y \sim \exp(0.13 \times 4\pi) \sim 5$.

The logarithmic divergence makes the integral (38) over A_B problematic, but the same truncation as used in section 3.1 for nodal lines leads to the following mean nodal number, expressed in terms of k and n:

$$
\begin{aligned}
\langle N \rangle &= \frac{A_B k^2}{4\pi} + \frac{L_B k}{16\pi^2} \log(k\sqrt{A_B}) + \mathrm{O}(k) \\
&= n + \frac{L_B}{16\pi^{3/2}\sqrt{A_B}} \sqrt{n} \log n + \mathrm{O}(\sqrt{n}).
\end{aligned} \tag{45}
$$

The positive excess of nodal points resulting from the influence of the boundary, in both the Dirichlet and Neumann cases, is surprising. It contradicts and supersedes the conjecture in Berry and Robnik (1986a). This was based on a semiquantitative argument incorporating only the depletion near the boundary, and neglecting the long-range excess embodied in (42) and (44).

4.2. Fluctuation in number of nodal points

To estimate these fluctuations, it suffices, as with nodal line lengths, to use the isotropic Gaussian random function ψ, defined by (2) and (6). The fluctuations can be calculated from

$$\delta N \equiv \sqrt{\langle (N - \langle N \rangle)^2 \rangle} = \sqrt{\langle N^2 \rangle - \langle N \rangle^2}. \tag{46}$$

The result is

$$\langle N^2 \rangle = \left(\frac{k^2}{4\pi}\right)^2 \iint_{A_B} \mathrm{d}\boldsymbol{r}_A \iint_{A_B} \mathrm{d}\boldsymbol{r}_B \; g_P(|\boldsymbol{R}_A - \boldsymbol{R}_B|), \tag{47}$$

where

$$g_P(|\mathbf{R}_A - \mathbf{R}_B|) = 16\pi^2 \langle \delta(u(\mathbf{r}_A)) \delta(u(\mathbf{r}_B)) \delta(v(\mathbf{r}_A)) \delta(v(\mathbf{r}_B))$$
$$\times |\nabla_R u(\mathbf{r}_A) \times \nabla_R v(\mathbf{r}_A)||\nabla_R u(\mathbf{r}_B) \times \nabla_R v(\mathbf{r}_B)|\rangle. \tag{48}$$

$g_P(R)$ is the planar correlation function between nodal points. It was calculated in section 4e of Berry and Dennis (2000), in terms of an integral, whose explicit representation in terms of elliptic integrals was given by Dennis (2001). As with the corresponding quantity (25) for nodal line lengths, only the large-R asymptotics is required in order to estimate the fluctuations, and this can be calculated to be

$$g_P(R) = 1 + \frac{4\sin(2R)}{\pi R} + \frac{11}{8\pi^2 R^2} + O\left(\frac{\sin(2R+\mu)}{R^2}\right). \tag{49}$$

As in the case of nodal line lengths, the nonoscillatory term is of order R^{-2} rather than R^{-1}, because of an unanticipated cancellation. In the integral (47), this leads to a divergence, whose natural truncation gives the estimate

$$(\delta N)^2 \approx \frac{11 A_B k^2}{64\pi^3} \log(k\sqrt{A_B}), \tag{50}$$

or, in terms of n rather than k,

$$\delta N \approx \frac{1}{4\pi}\sqrt{\frac{11}{2} n \log n}. \tag{51}$$

Again this is smaller than the boundary contribution to the mean nodal number (45).

The theory of this section has been concerned with the number of nodal points regardless of their associated signs, i.e. topological charges (+1 for a phase change $+2\pi$ in a positive circuit of the zeros, -1 for a phase change -2π). Interesting long-range effects in the charge correlation function, given by (48) without the modulus signs, and interpretable in terms of screening, have been described by Freund and Wilkinson (1998), Berry and Dennis (2000) and Dennis (2001).

5. Concluding remarks

The main theoretical innovation has been the use of a Gaussian random function locally adapted to satisfy billiard boundary conditions. This enables perimeter corrections to be determined up to the leading (logarithmic) order, but is insufficient to determine the associated constants. A possible extension would be to choose random functions adapted not to a straight boundary but to a circular one. This would enable the development of Gaussian random models satisfying boundary conditions to higher order in k, and possibly determining these constants. However, these circular waves are superpositions of Bessel functions rather than plane waves, and the corresponding analysis would be more complicated. Looking further ahead, it might be possible to generate superpositions matching the boundary conditions to arbitrarily high order, and so generate nodal (and other) statistics including more boundary corrections.

A surprising outcome of this work is the long-range behaviour of the nodal line and point densities as functions of distance y from the boundary. This leads to the predictions of nodal excesses (negative for lines (equations (16), (18), (19)), positive for points (equations (42), (44), (45)) growing logarithmically with y. Other unexpected logarithms occur in the fluctuations of nodal line lengths ((28), (29)) and numbers of nodal points ((50), (51)). Perhaps these are related to other long-range structures in Gaussian random superpositions, for example the lines of high intensity ('scarlets') observed and described by O'Connor et al (1987).

The observation, at least in numerical experiments, of the nodal line curvature statistics of section 3.3 should not be too difficult. It should also be possible to study the depletion of nodal lines and points near boundaries, and test the density functions in figures 2 and 4. However, detecting the logarithmic perimeter and fluctuation effects might present a challenge to numerical analysis, since these might be easily masked by the local depletion. The most promising strategy would seem to be to study the Neumann cases, where the constants (equations (19) and (44)) are smaller, so the logarithms get established closer to the boundary.

Acknowledgments

Appendix. Mixed boundary conditions

The most general local Hermitian (Robin) boundary condition is, for a real wavefunction with boundary $y = 0$,

$$\cos(\alpha)u(0, x) + \frac{\sin(\alpha)}{k}u_y(0, x) = 0, \tag{A.1}$$

where α is a real angle between 0 and π, with $\alpha = 0$ corresponding to the Dirichlet condition and $\alpha = \pi/2$ corresponding to the Neumann condition. For complex waves ψ, the same relation holds. The boundary-adapted Gaussian random function satisfying (A.1) and representing a superposition of isotropically distributed plane waves is the generalization of (7) and (8), easily calculated to be

$$u(\boldsymbol{R}) = \frac{2}{\sqrt{J}} \sum_{j=0}^{J} \sin(Y \sin \theta_j - \tan^{-1}(\sin \theta_j \tan \alpha)) \cos(X \cos \theta_j + \phi_j)$$

$$= \frac{2}{\sqrt{J}} \sum_{j=0}^{J} \frac{\cos \alpha \sin(Y \sin \theta_j) - \sin \theta_j \sin \alpha \cos(Y \sin \theta_j)}{\sqrt{\cos^2 \alpha + \sin^2 \alpha \sin^2 \theta}} \cos(X \cos \theta_j + \phi_j). \tag{A.2}$$

The correlations involving u and its derivatives, generalizing B, D_x, D_y and K in (9) and (10), cannot be evaluated in closed form, but they are easy to calculate numerically, and their large-Y asymptotics can be calculated analytically. These correlations appear in the density $\rho_L(Y)$ (equation (14)) for nodal line length, and its equivalent $\rho_P(Y)$ (equation (40)) for nodal points.

For nodal lines, the asymptotic form, generalizing (15) and (17), is

$$\rho_L(Y) = 1 + \frac{\cos(2Y - 2\alpha - \frac{1}{4}\pi)}{\sqrt{\pi Y}} - \frac{1}{32\pi Y} + o\left(\frac{1}{Y}\right) \qquad \text{as } Y \to \infty. \tag{A.3}$$

The coefficient of the nonoscillatory correction term is independent of α.

For nodal points, the asymptotic form, generalizing (41) and (43), is

$$\rho_P(Y) = 1 + \frac{2\cos(2Y - 2\alpha - \frac{1}{4}\pi)}{\sqrt{\pi Y}} + \frac{1}{4\pi Y} + o\left(\frac{1}{Y}\right) \qquad \text{as } Y \to \infty. \tag{A.4}$$

Again, the coefficient of the nonoscillatory correction term is independent of α.

The nodal densities near $Y = 0$ display interesting structure when α is small and positive; this will be described elsewhere.

References

Balian R and Bloch C 1970 Distribution of eigenfrequencies for the wave equation in a finite domain: I. *Ann. Phys., NY* **60** 401–7

Berry M V 1977 Regular and irregular semiclassical wave functions *J. Phys. A: Math. Gen.* **10** 2083–91

Berry M V 1978 Disruption of wavefronts: statistics of dislocations in incoherent Gaussian random waves *J. Phys. A: Math. Gen.* **11** 27–37

Berry M V 1981 *Les Houches Lecture Series Session 35* ed R Balian, M Kléman and J-P Poirier (Amsterdam: North-Holland) pp 453–543

Berry M V 1983 *Les Houches Lecture Series* vol 36, ed G Iooss, R H G Helleman and R Stora (Amsterdam: North-Holland) pp 171–271

Berry M V and Dennis M R 2000 Phase singularities in isotropic random waves *Proc. R. Soc.* A **456** 2059–79

Berry M V and Robnik M 1986a Quantum states without time-reversal symmetry: wavefront dislocations in a nonintegrable Aharonov–Bohm billiard *J. Phys. A: Math. Gen.* **19** 1365–72

Berry M V and Robnik M 1986b Statistics of energy levels without time-reversal symmetry: Aharonov–Bohm chaotic billiards *J. Phys. A: Math. Gen.* **19** 649–68

Bies W E and Heller E J 2002 Nodal structure of chaotic eigenfunctions *J. Phys. A: Math. Gen.* submitted

Blum G, Gnutzmann S and Smilansky U 2002 Nodal domain statistics—a criterion for quantum chaos *Phys. Rev. Lett.* **88** 114101

Bogomolny E and Schmit C 2002 Percolation model for nodal domains of chaotic wavefunctions *Phys. Rev.* E submitted

Dennis M 2001 *Singular Optics 2000* vol 4403, ed M Soskin (Alushta, Crimea: SPIE) pp 13–23

Freund I and Wilkinson M 1998 Critical-point screening in random wave fields *J. Opt. Soc. Am.* A **15** 2892–902

McDonald S W and Kaufman A N 1988 Wave chaos in the stadium: statistical properties of short-wave solutions of the Helmholtz equation *Phys. Rev.* A **37** 3067–86

Nye J F and Berry M V 1974 Dislocations in wave trains *Proc. R. Soc.* A **336** 165–90

O'Connor P, Gehler J and Heller E J 1987 Properties of random superpositions of plane waves *Phys. Rev. Lett.* **58** 1296–9

Rice S O 1944 Mathematical analysis of random noise *Bell Syst. Tech. J.* **23** 282–332

Rice S O 1945 Mathematical analysis of random noise *Bell Syst. Tech. J.* **24** 46–156

Saichev A I, Ishio H, Sadreev A F and Berggren K-F 2002 Current statistics for quantum transport through two-dimensional open chaotic billiards *J. Phys. A: Math. Gen.* **35** L87–93

Soskin M S E 1998 Singular optics *SPIE Proc.* **3487**

Soskin M S and Vasnetsov M V 2001a Singular optics *Prog. Opt.* **42** 219–76

Soskin M S and Vasnetsov M V (ed) 2001b Singular optics (optical vortices): fundamentals and applications *SPIE Proc.* **4403**

Struik D J 1950 *Lectures on Classical Differential Geometry* (Reading, MA: Addison-Wesley)

Vasnetsov M and Staliunas K (eds) 1999 *Optical Vortices* (Commack, NY: Nova)